ACADEMIC PRESS

Available online at www.sciencedirect.com
SCIENCE DIRECT®

NeuroImage

NeuroImage 19 (2003) 1395–1404

www.elsevier.com/locate/ynimg

Simultaneous ERP and fMRI of the auditory cortex in a passive oddball paradigm

Einat Liebenthal,[a,*] Michael L. Ellingson,[b] Marianna V. Spanaki,[a] Thomas E. Prieto,[a] Kristina M. Ropella,[b] and Jeffrey R. Binder[a]

[a] *Department of Neurology, Medical College of Wisconsin, Milwaukee, WI 53226, USA*
[b] *Department of Biomedical Engineering, Marquette University, Milwaukee, WI 53201, USA*

Received 23 October 2002; revised 13 March 2003; accepted 8 April 2003

Abstract

Infrequent occurrences of a deviant sound within a sequence of repetitive standard sounds elicit the automatic mismatch negativity (MMN) event-related potential (ERP). The main MMN generators are located in the superior temporal cortex, but their number, precise location, and temporal sequence of activation remain unclear. In this study, ERP and functional magnetic resonance imaging (fMRI) data were obtained simultaneously during a passive frequency oddball paradigm. There were three conditions, a STANDARD, a SMALL deviant, and a LARGE deviant. A clustered image acquisition technique was applied to prevent contamination of the fMRI data by the acoustic noise of the scanner and to limit contamination of the electroencephalogram (EEG) by the gradient-switching artifact. The ERP data were used to identify areas in which the blood oxygenation (BOLD) signal varied with the magnitude of the negativity in each condition. A significant ERP MMN was obtained, with larger peaks to LARGE deviants and with frontocentral scalp distribution, consistent with the MMN reported outside the magnetic field. This result validates the experimental procedures for simultaneous ERP/fMRI of the auditory cortex. Main foci of increased BOLD signal were observed in the right superior temporal gyrus [STG; Brodmann area (BA) 22] and right superior temporal plane (STP; BA 41 and 42). The imaging results provide new information supporting the idea that generators in the right lateral aspect of the STG are implicated in processes of frequency deviant detection, in addition to generators in the right and left STP.

Introduction

Focal changes in blood oxygenation level-dependent (BOLD) signal recorded with functional magnetic resonance imaging (fMRI) allow fine spatial localization of the metabolic response induced by neural activation, but do not reflect neural activation directly and cannot reveal its temporal sequence. Conversely, event-related potentials (ERPs) give fine temporal resolution of neural activity from sources capable of generating far-field potentials, but have poor spatial resolution. The combination of these techniques may allow improved localization of neural generators as well as enhanced temporal resolution of BOLD activation foci.

Simultaneous ERP/fMRI is particularly valuable for obtaining perfect correspondence of experimental conditions and cognitive state between the two types of recordings. For instance, in the present auditory experiment, the level and spectrum of the acoustic noise of the scanner at the subjects' ears in the magnet, and the subjects' attention state—two factors potentially affecting the recorded response—would be impossible to accurately match if the ERP and fMRI recordings were conducted separately. Simultaneous recordings are technically challenging, mainly because they involve extracting the small ERP signal from the increased background noise caused by the magnetic field. The magnetic field introduces a ballistocardiogram artifact (BA), which is induced by motion of closed electrical loops (formed by the scalp electrodes, leads, and skin) in a non-uniform magnetic field and is time-locked to the heartbeat (Schomer et al., 2000). The BA can reach amplitudes 100 times larger than those of the ERPs and so must be removed

* Corresponding author. Department of Neurology, Medical College of Wisconsin, 8701 Watertown Plank Road, Milwaukee, WI 53226, USA. Fax: +1-414-456-6562.
E-mail address: einatl@mcw.edu (E. Liebenthal).

1053-8119/03/$ – see front matter © 2003 Elsevier Science (USA). All rights reserved.
doi:10.1016/S1053-8119(03)00228-3

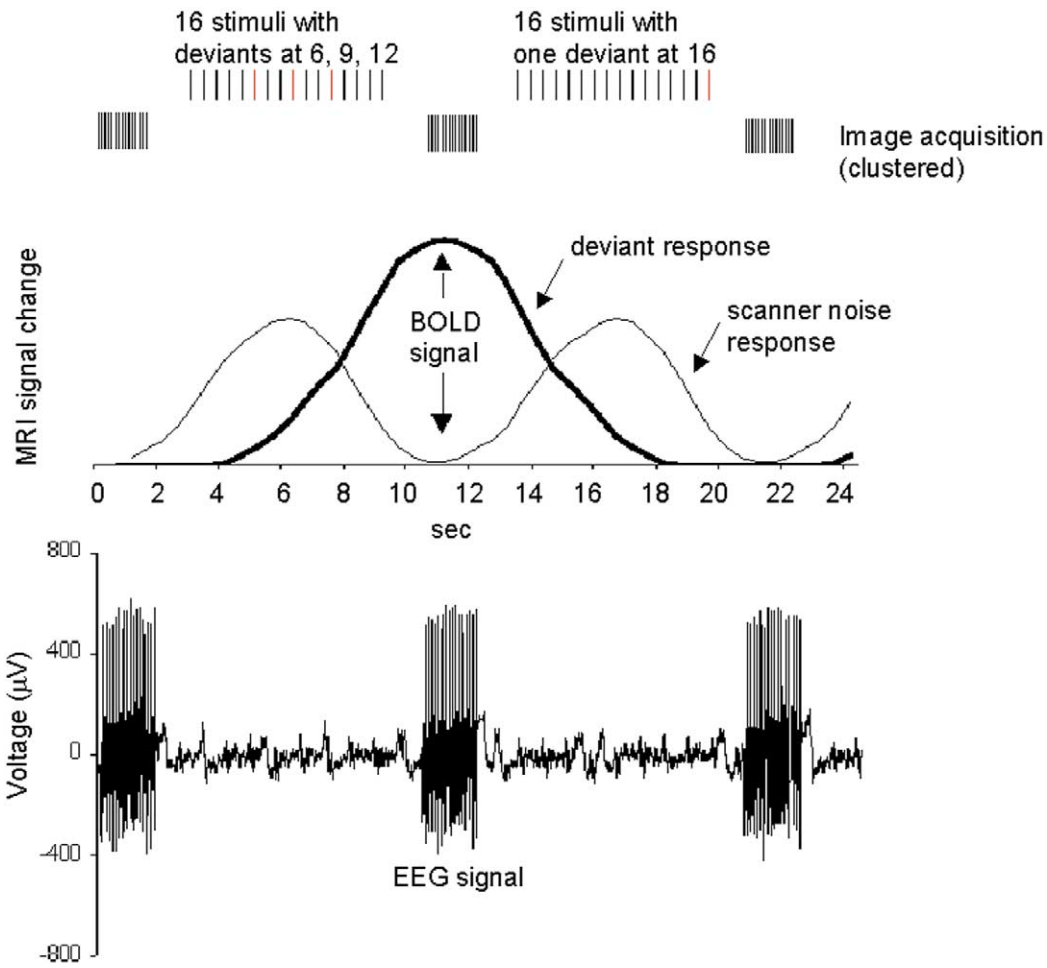

Fig. 1. Experimental design. An epoch of 24 s, including 2 intervals of stimulus presentation (top row) and 3 intervals of clustered image acquisitions (2nd row), as well as a model of the blood oxygenation level-dependent (BOLD) signal evoked by the scanner noise and the stimulus sequence (3rd row) and a sample electroencephalogram (EEG) recorded during this epoch (4th row), are shown. Auditory stimulation, presented in periods between image acquisitions, consisted of alternating 8-s sequences of 16 tones with 1 deviant in position 16 (STANDARD condition) or with 3 embedded deviants in positions 6, 9, and 12, or 6, 10, and 13 (DEVIANT conditions). Images were collected every 10.5 s, at the peak of the BOLD response to the deviants in the DEVIANT sequences. The EEG signal was collected continuously, but the analysis was restricted to intervals between image acquisitions, when stimuli were presented.

from the electroencephalogram (EEG). Visual ERPs have successfully been recorded during fMRI (Bonmassar et al., 1999, 2001; Kruggel et al., 2000, 2001). No studies using auditory ERP recording during MRI scanning have yet been reported.

The aim of the present study was to develop an experimental procedure for simultaneous ERP/fMRI recordings of the auditory cortex during a passive oddball paradigm to describe the neural generators involved in specific aspects of auditory analysis. Infrequent occurrences of a deviant sound within a sequence of repetitive standard sounds elicit an automatic brain response, observed as a mismatch negativity (MMN) in scalp-recorded ERPs (Naatanen, 1992). The main MMN neural generators are thought to be located in the left and right auditory cortices in the superior temporal cortex (Alho, 1995), but the number of generators, their precise location, and temporal sequence of activation remain unclear. Furthermore, different auditory cortex sources may be involved in generation of the MMN to deviations in different auditory attributes (Giard et al., 1995), making this component a sensitive probe of neurophysiological substrates subserving specific aspects of auditory analysis.

In this study, the neural generators underlying automatic detection of a frequency deviant were considered. Two levels of deviancy from the STANDARD 1000 Hz tone were used, a SMALL deviant of 1250 Hz and a LARGE deviant of 1500 Hz. Simultaneous ERP/fMRI recordings of the standard and deviant evoked activities were obtained in a 1.5T MRI scanner. A clustered image acquisition technique was applied to prevent contamination of the BOLD response by the acoustic noise of the scanner and to limit the epochs of contamination of the EEG by the gradient switching occurring during image acquisition. The MMN peak amplitude is known to increase as a function of the extent of deviancy (Lang et al., 1990; Scherg et al., 1989; Tiitinen et al., 1994). The amplitudes of the ERP evoked by the STANDARD, the SMALL, and the LARGE deviants were used to identify brain

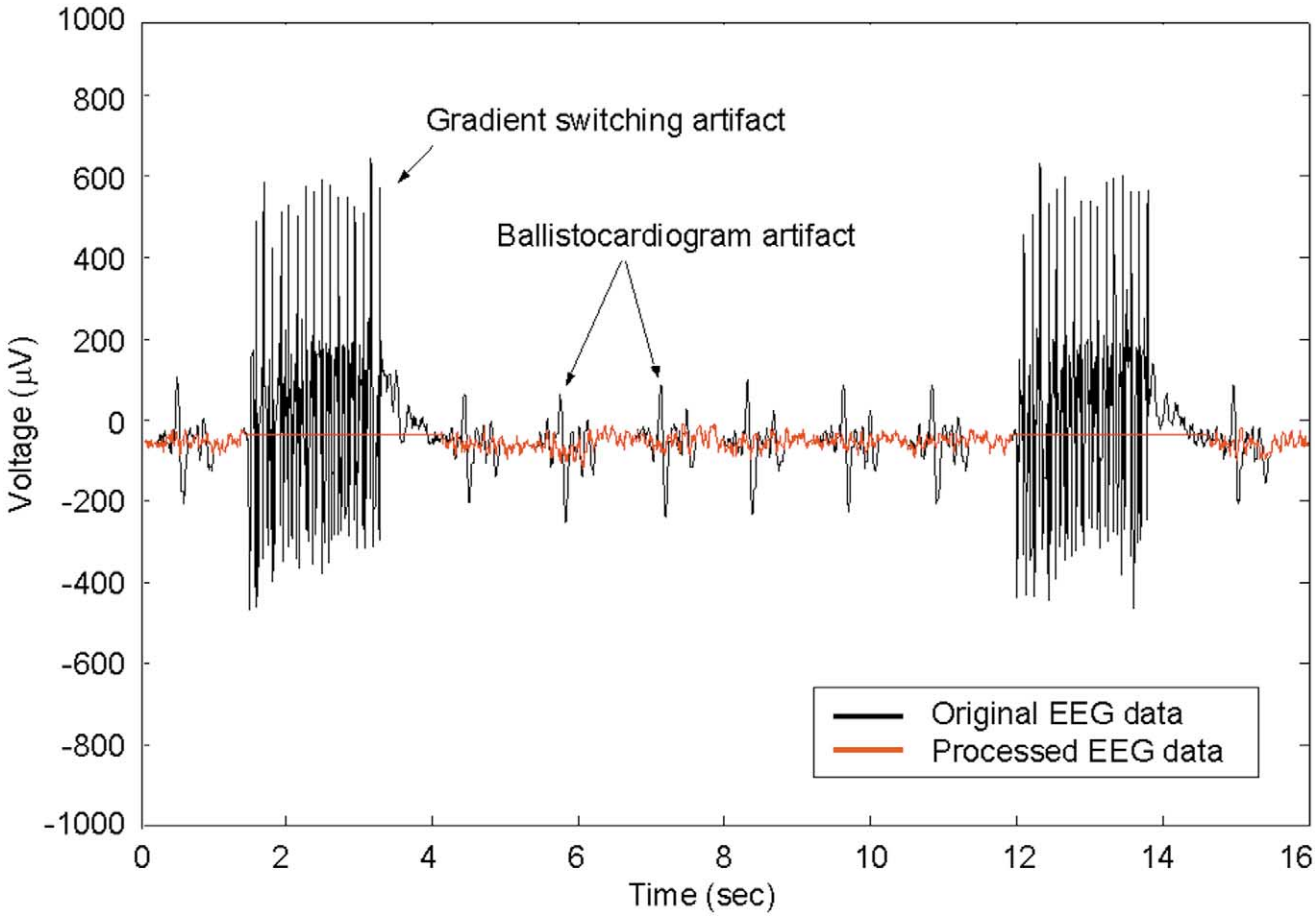

Fig. 2. Electro encephalographic (EEG) recordings before and after artifact reduction. The black trace represents the original EEG with the gradient-switching artifact and the ballistocardiogram artifact (BA). The red trace represents the processed EEG after zeroing of periods of gradient-switching artifact and after reduction of the BA.

areas in which BOLD activation varied with the magnitude of the evoked negativity.

Methods

Subjects

Simultaneous ERP/fMRI recordings were obtained from 11 subjects (6 females), 21–49 years old, without auditory or neurological complaints. Data from 2 subjects were excluded due to excessive movement artifacts in the EEG (less than 190 ERP responses available per deviant condition). Data from 2 other subjects were excluded because no negativity was observed within the MMN time range. The final group (7 subjects) included 4 females and ranged 20–49 years in age. Informed consent was obtained from each subject prior to the experiment, in accordance with the Medical College of Wisconsin policies and the Froedtert Memorial Lutheran Hospital Institutional Review Board (FMLH#01-058).

Auditory stimulation

Auditory stimulation was delivered binaurally through plastic tubing attached to foam earplugs using a commercial system (Magnacoustics Inc., Atlantic Beach, NY) that is MRI and EEG compatible. The tubes introduced a constant delay of 9 ms in sound presentation at the ears in the range of frequencies used in this study. Stimuli consisted of alternating 8-s sequences of 16 tones, composed mostly of 1000 Hz pure tones with only one deviant in position 16 (STANDARD condition) or including three embedded deviants of 1250 Hz (SMALL deviant condition) or 1500 Hz (LARGE deviant condition) in positions 6, 9, and 12, or 6, 10, and 13. The probability of the deviant in the deviant sequences was 0.19. The deviants were positioned such that their estimated combined BOLD response peaked during image acquisition. In the standard sequences, the deviant in position 16 varied semirandomly between SMALL and LARGE such that there were 50% deviants of each type. The rationale for adding a deviant at the end of the STANDARD sequences was to increase the number of recorded ERP deviant responses

(by 54/deviant condition) without increasing the recording time. Owing to the lag in the BOLD response, the response to this final deviant peaked between image acquisitions and did not contaminate the STANDARD BOLD response. A total of 108 sequences of each type were presented over six separate runs, bringing the total number of deviants of each type presented throughout the experiment to 378. Thus, 108 images and 378 ERP responses were collected per experimental condition. The order of presentation of the sequences of each type was randomized within a run except that every third sequence consisted of the STANDARD condition. The tones were 50 ms long and were presented at 2 Hz. The tone sequences were presented during the "quiet" periods between image acquisitions. The average output level of the tone sequences delivered at the ears was 89 dB SPL. The acoustic noise of the gradients during image acquisition was attenuated to an average level of 86 dB SPL by the protective foam earplugs and hence did not compromise the subjects' hearing. See Fig. 1 for details of the experimental design.

Task

Subjects were instructed to press a button at the onset of each image acquisition (indicated by the acoustic noise produced by the switching of gradients). The task was designed to maintain the subjects' state of arousal without drawing their attention to the tone sequences. Speed of response was not emphasized and responses occurring within the window of image acquisition (1800 ms) were considered correct. Response accuracy averaged 98.2% ($\pm$0.01% standard error) and the response time for correct responses averaged 484 ms ($\pm$49 ms standard error).

ERP recording

A 30-channel EEG was acquired using the fMRI-compatible Optilink acquisition system (Neuroscan, Inc., TX) in a continuous mode, and the Quik-Cap electrode positioning system (Neuroscan, Inc., TX). Electrode sites conformed to the International 10–20 System. Potentials recorded at each site were referenced to the tip of the nose. Vertical eye movements were monitored with bipolar recordings between sites above and below the left eye. The horizontal eye channels were altered to record electrocardiographic (ECG) activity between the standard V1 ECG lead and the left outer canthus. Interelectrode resistance was kept below 5 kΩ. Activity was recorded between 0.3 and 70 Hz and digitally sampled at 500 Hz per channel. Synchronization between the ERP and fMRI acquisition was achieved by a scanner-initiated trigger to the stimulus delivery system (Psyscope, Carnegie Mellon University) at the onset of every run. The stimulus delivery system in turn sent pulses to the Optilink system to tag the EEG at each stimulus event with millisecond accuracy.

BA reduction algorithm

The BA reduction method was similar to the method previously described by Allen et al. (1998) in that it was based on detection of QRS complexes from the ECG channel to provide timing information for the occurrences of the BA. In a first step, the gradient-switching periods were zeroed out in the ECG channel to allow for accurate detection of the QRS complexes. Second, a variation of Pan and Tompkins (1985) real-time QRS detection algorithm was implemented to detect the QRS complexes by analyzing the slope, amplitude, and width of the waveforms. The original ECG signal was bandpass filtered at 12.5–27.5 Hz to isolate the predominant QRS energy, and it was differentiated and squared to enhance the higher frequency components. A moving-window integrator was applied, and the integrated waveform was passed through a 30-point moving-average filter to determine a single peak for each QRS complex. The integrated signal was normalized and the amplitude threshold for detecting the QRS complexes was set to 40% of the median peak amplitude value for a 10-s section of ECG. This amplitude threshold was updated for each consecutive 10-s segment of ECG. The window width for BA template formation and reduction was set to 70% of the average period between heart beats. After the peaks of the integrated QRS complexes were detected and their temporal locations determined, windows of data encompassing these temporal locations in the EEG channels were used to create a template of the BA artifact. The artifact template was determined by taking the previous 10 artifact segments and finding the median value on a point-by-point basis. The artifact template was offset and scaled in amplitude to each section of EEG data containing the BA artifact using least-squares minimization, and it was subsequently subtracted from the EEG. See Fig. 2 for an example of EEG recordings before and after artifact reduction.

ERP analysis

Within-subject analysis consisted of creating epochs of -100 to $+500$ ms from each tone onset, bandpass filtering the data at 1–30 Hz (Butterworth squared filter, 24 dB/oct rolloff), baseline correcting each epoch by removing the mean voltage value of the whole sweep, and rejecting epochs with voltage values exceeding ± 100 μV. The remaining epochs were then sorted and averaged according to stimulus type (STANDARD, SMALL deviant, LARGE deviant). The average of STANDARD responses was restricted to responses to standard tones occurring in standard sequences in the same positions occupied by deviants in the deviant sequences (positions 6, 9, 10, 12, 13, and 15[1]). This procedure was meant to avoid possible confounds from an effect

[1] Responses to standards in position 15 were included in the STANDARD average to match the responses to the deviants occurring in position 16 in the standard sequences and included in the DEVIANT averages.

of the order of the tones in the sound sequences. In addition, analysis of responses to the first tones in the STANDARD sequences was avoided to prevent contamination of the data by the transient signal caused in the EEG by the switching of the scanner gradients and lasting up to 1.5 s after image acquisition. Subjects with less than 190 artifact-free ERP deviant responses per experimental condition were excluded from the analysis.[2] This minimum number of responses was chosen because it allowed to include most subjects and to obtain a reasonable signal-to-noise ratio through averaging (Lang et al., 1995). Each average was again baseline corrected by subtracting the mean voltage of the prestimulus period from the average. Individual difference waveforms in each deviant condition were computed by subtracting from the average response to the deviant stimuli in the deviant sequences, the average responses to the standard stimuli in the same positions in the standard sequences. Grand means of the difference waveforms in each deviant condition were subsequently created. A temporal window of ± 25 ms from the peak of the largest negativity in the grand-mean waveforms (109–159 ms) was used to compute individual amplitude averages for the standard and for the deviant waveforms within this window. A repeated-measures analysis of variance (ANOVA) with factors of stimulus type (standard; deviant) and electrode site as a repeated measure (FZ, F3, F4, FC3, FC4, FP1, FP2, M1, M2) was conducted on the windowed amplitude averages to test for main effects of stimulus type, i.e., test for presence of an MMN. The presence of the MMN was tested at the frontal electrode sites where the MMN is most prominent and at the mastoids where it reverses in polarity (Vaughan and Ritter, 1970; Alho et al., 1986). *t* tests for dependent samples were applied to test for peak amplitude and peak latency differences at FZ between the two deviant conditions. Reported latencies were corrected to represent the delay from sound presentation at the subjects' ears.

Image acquisition and analysis

Images were acquired on a 1.5-T GE Signa scanner (GE Medical Systems, Milwaukee, WI). Functional data consisted of T2*-weighted, gradient-echo, echoplanar images (TE = 40 ms, flip angle = 90°, NEX = 1), obtained using clustered acquisition (acquisition time = 1800 ms) at 10.5-intervals to avoid perceptual masking of the test items or contamination of the data by the acoustic noise of the scanner (Edmister, et al., 1999). The images were reconstructed from 16 axially oriented contiguous slices with $3.75 \times 3.75 \times 4$-mm voxel dimensions. Slice coverage was centered obliquely around the temporal lobes and varied by a few millimeters from subject to subject, such that it included most of the temporal lobes (except for the most anterior and ventral tip of the superior, middle, and inferior temporal gyri), part of the frontal and parietal lobes (including all the inferior frontal gyrus and missing the dorsal portions of the middle and superior frontal gyri and the dorsal portion of the parietal lobe), and the occipital lobe. High-resolution anatomical images of the entire brain were obtained by using a 3D spoiled gradient-echo sequence (SPGR, GE Medical systems, with $0.9 \times 0.9 \times 1.2$-mm voxel dimensions.

Image analysis was done with the AFNI software package (Cox, 1996). Within-subject analysis consisted of spatial coregistration of each functional volume to the last steady-state functional volume acquired before the anatomical scan, using an iterative voxelwise least-squares approach (Cox and Jesmanowicz, 1999) to minimize head motion artifacts. All 108 co-registered volumes in each experimental condition were subsequently used to create individual statistical parametric maps. A correlation analysis to detect brain voxels for which BOLD activation varied with the windowed amplitude averages at FZ in the different conditions (STANDARD, SMALL deviant, and LARGE deviant) was applied to create the functional maps. The signs of the amplitude values were inverted such that a positive correlation would indicate an increase in the BOLD signal with the magnitude of the negativity. Individual anatomical scans and statistical maps were projected into standard stereotaxic space (Talairach and Tournoux, 1988). The statistical maps were smoothed with a Gaussian filter measuring 4-mm full-width-half-maximum to compensate for individual variation in anatomy across subjects. The correlation values were transformed into *z*-scores and the statistical maps were merged across subjects by averaging the *z*-scores at each voxel. Randomization testing was used to determine the threshold *z*-values for rejecting the null hypothesis in the group maps (Bullmore et al., 1996). Average *z*-values of 0.03 or larger were considered significant (uncorrected voxelwise $P < 10^{-5}$). Activation foci smaller than 300 μl were removed, which lowered the probability of false positives to $P < 10^{-8}$ as determined by Monte Carlo simulation using the "AlphaSim" module in AFNI (Ward, 2000). Activation peaks, separated by at least 10 mm, were computed by using the Maxima AFNI option.

Results

ERPs

The grand mean difference waveforms to SMALL and LARGE deviants are shown in Fig. 3. ANOVA with factors of stimulus type (standard; deviant) and electrode site as a repeated measure (FZ, F3, F4, FC3, FC4, FP1, FP2, M1, M2) conducted on the windowed amplitude averages confirmed that an ERP MMN was recorded in both the LARGE and the SMALL deviant conditions [LARGE: $F(1,12) = 11.01$, $P < 0.01$; SMALL; $F(1,12) = 5.92$; $P < 0.03$]. Planned

[2] The numbers of valid deviant trials for the two subjects excluded from the study based on this criterion were 91 and 110.

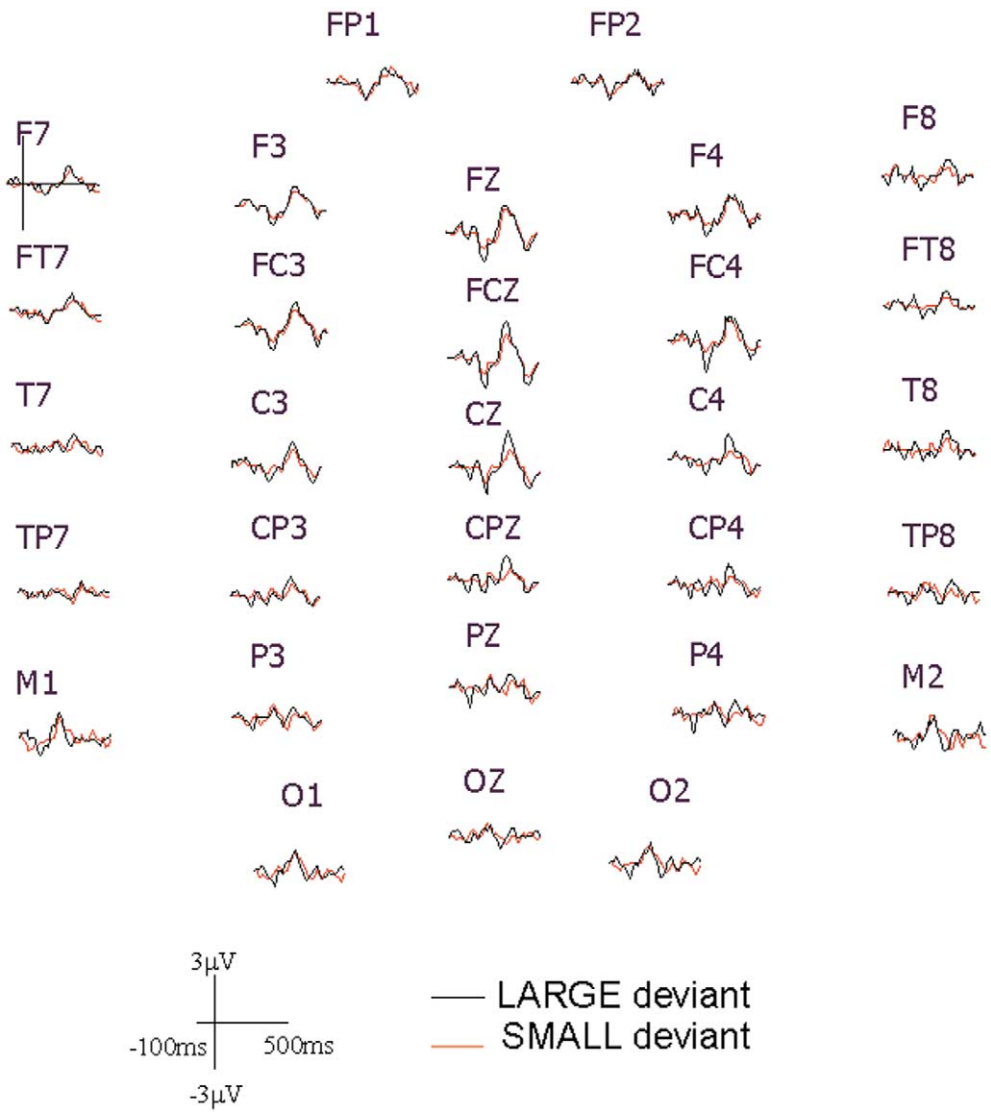

Fig. 3. Group average difference waveforms in the SMALL (red trace) and LARGE (black trace) deviant conditions, at the 30 scalp-recording sites and at −100 to +500 ms from deviant presentation. The mismatch negativity (MMN) is observed as a negativity peaking at approximately 140 ms over frontocentral sites (FZ and adjacent sites) and inverting in polarity over the mastoids (M1, M2).

comparisons confirmed that the MMN windowed average values were more negative in the deviant relative to the standard condition at the frontal sites (FZ, F3, F4, FC3, FC4, FP1, FP2) and were more positive at the left mastoid (M1) in both LARGE and SMALL deviant conditions. At the right mastoid (M2), the effect was significant for the SMALL deviant condition, but only approached significance in the LARGE deviant condition (see Table 1).

t tests for dependent samples were conducted on the peak amplitude and peak latency of the difference waveform at FZ to test for significant differences between the LARGE and SMALL deviant condition. The average peak amplitudes (and standard errors) at FZ were −3.2 (±0.8) μV and −2.0 (±0.4) μV and the average peak latencies were 131 (±6) ms and 134 (±7) ms for the LARGE and SMALL deviant conditions, respectively. These tests revealed that the MMN peak amplitudes had significantly more negative values in the LARGE relative to the SMALL deviant condition (FZ: $t = -3.15$; $P < 0.02$), but the peak latencies were not statistically different between the conditions (FZ: $t = -0.47$; $P < 0.66$).

Fig. 4 shows the voltage distribution over the scalp during the MMN time window, in both deviant conditions. The negativity is greater in the LARGE deviant condition at all time points. In both conditions, the negativity was most prominent over the frontocentral region, and there was a reversal of polarity at the mastoids. In addition, the negativity was more pronounced over the right hemisphere.

fMRI

A correlation analysis was applied within-subject to detect brain voxels for which BOLD activation varied with the windowed amplitude averages at FZ in the different conditions (STANDARD, SMALL deviant, LARGE deviant). These am-

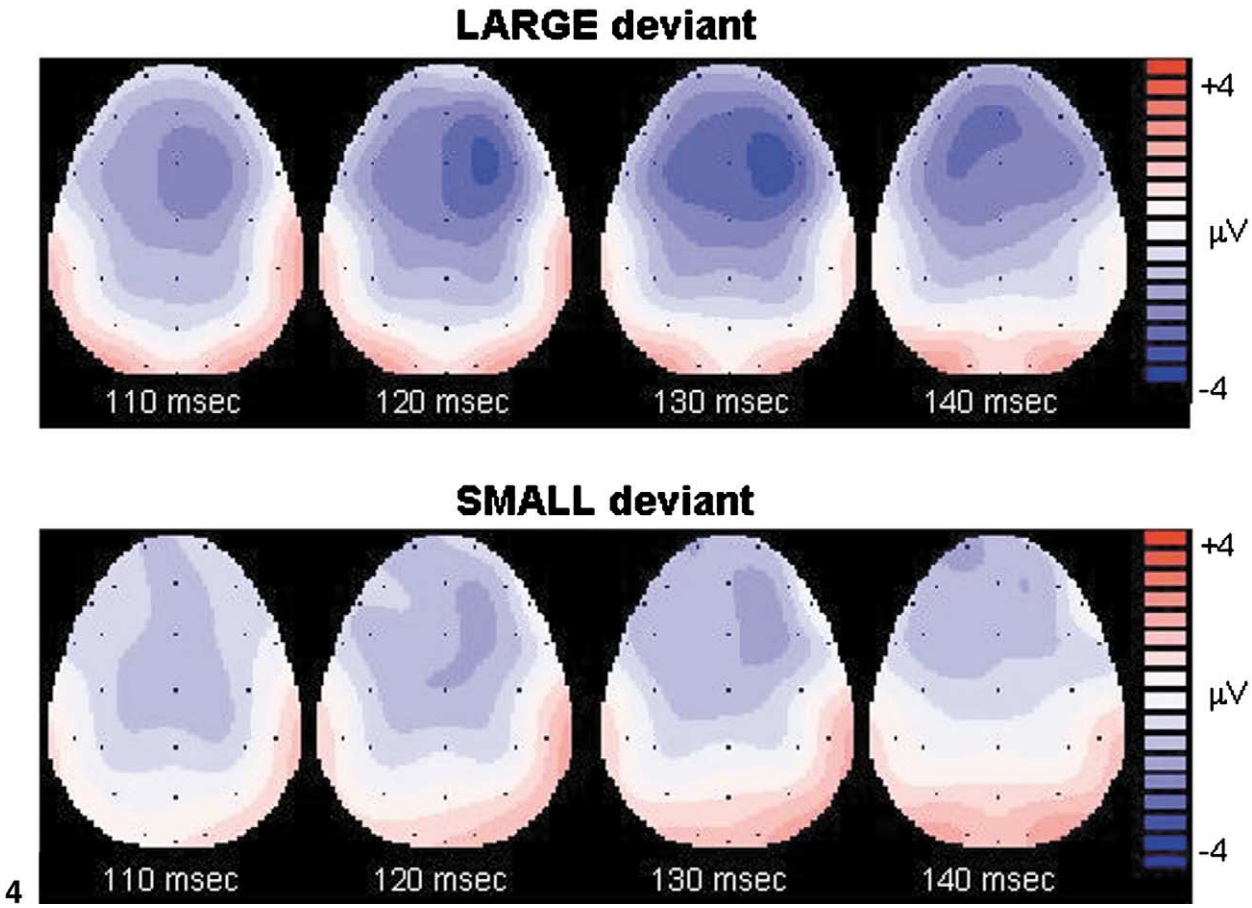

4

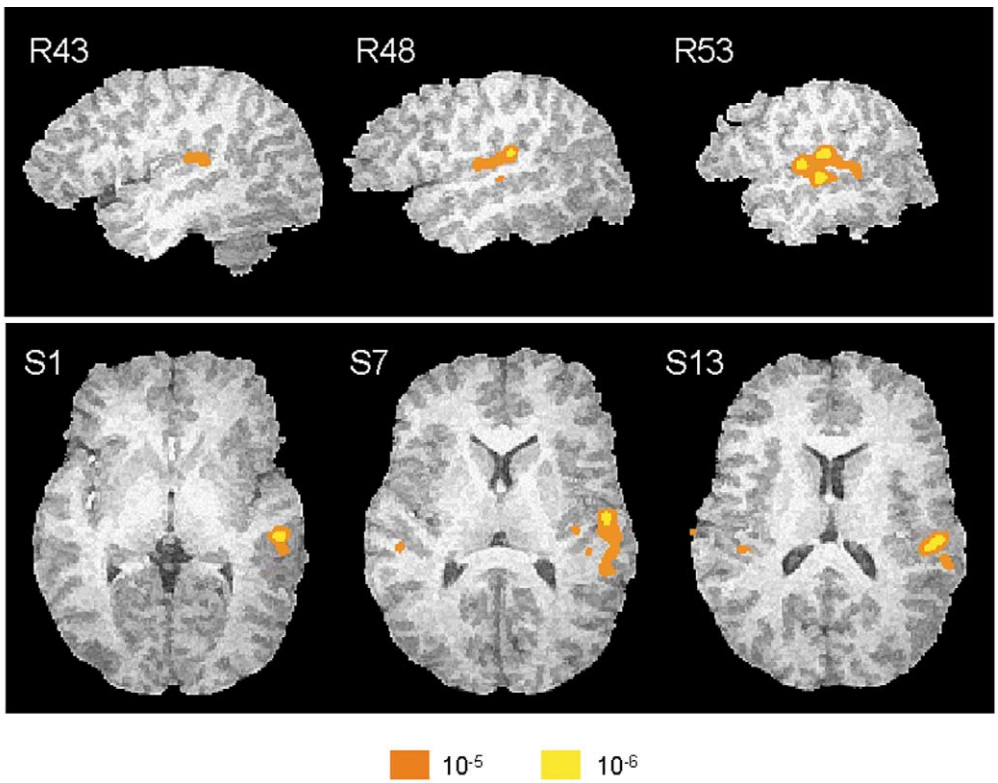

5

Fig. 4. Voltage distribution over the scalp during the mismatch negativity (MMN) time window, in the LARGE (upper graph) and the SMALL (lower graph) deviant conditions.

Fig. 5. Statistical parametric maps of activation correlated with the magnitude of the event-related potential (ERP) negativity during the mismatch negativity (MMN) temporal window, collapsed across subjects. The stereotaxic *x*-coordinate and lateralization relative to the AC-PC line (R = Right) of each sagittal section (top row) and the stereotaxic *z*-coordinate and level relative to the AC-PC line (S = Superior) of each axial section (bottom row) are given. Color coding indicates uncorrected voxelwise *P* values.

Table 1
Mean amplitude values (and standard errors in parentheses) of the ERP waveforms during the MMN window in response to standards and small and large deviants[a]

Electrode site	Average voltage in MMN window (μV)			F values	
	STANDARD	SMALL deviant	LARGE deviant	SMALL deviant	LARGE deviant
FZ	+0.25 (0.24)	−1.25 (0.44)	−2.18 (0.51)	9.11[b]	18.82[b]
F3	+0.15 (0.16)	−1.27 (0.45)	−1.74 (0.47)	8.74[b]	14.50[b]
F4	+0.32 (0.22)	−1.07 (0.48)	−1.76 (0.54)	6.90[b]	12.70[b]
FC3	+0.14 (0.17)	−1.20 (0.50)	−1.91 (0.5)	6.27[b]	13.96[b]
FC4	+0.11 (0.20)	−1.15 (0.54)	−2.36 (0.66)	4.71[b]	12.67[b]
FP1	+0.68 (0.30)	−1.25 (0.41)	−1.10 (0.69)	14.54[b]	5.58[b]
FP2	+0.80 (0.21)	−0.81 (0.40)	−0.97 (0.48)	12.54[b]	11.40[b]
M1	−0.53 (0.34)	+0.40 (0.25)	+0.93 (0.15)	4.98[b]	15.05[b]
M2	−0.74 (0.48)	+0.92 (0.43)	+0.50 (0.43)	6.60[b]	3.68

[a] F values are given for planned comparisons of average amplitude between each deviant condition and the standard condition, at each electrode site. ERP, event-related potential; MMN, mismatch negativity.
[b] Indicates F values that were significant at $P < 0.05$.

plitude values are given in Table 1. The main foci of increased BOLD activation correlated with the magnitude of the negativity (Fig. 5 and Table 2) were observed in the right superior temporal gyrus (STG), ventrally, bordering the superior temporal sulcus (BA 22), and on the right superior temporal plane (STP) in the planum temporale (PT; BA 42). Additional smaller peaks were located in the right posterior STG, the right and left Heschl's gyrus (HG; BA 41), the left PT (BA 42), and the left STG (BA 22).

Discussion

A significant ERP MMN to frequency deviants in an oddball sequence was obtained during simultaneous ERP/fMRI. The larger MMN peaks obtained in the LARGE deviant condition and the frontocentral scalp distribution with a polarity reversal at the mastoids were comparable to the features of the MMN reported outside the magnetic field (Scherg et al., 1989; Naatanen, 1992; Lang et al., 1990; Tiitinen et al., 1994). These results demonstrate that a typical ERP MMN can be obtained in the scanner despite the intermittent acoustic noise produced by image acquisition between trains of tone stimuli. The results also validate the algorithm that was developed to reduce the ballistocardiogram artifact.[3]

[3] In a second experiment to be reported separately, ERP recordings from a subset of the subjects participating in this experiment and to the same auditory stimuli were obtained in a mock scanner. A recording of the acoustic noise of the scanner was presented during the intervals when image acquisition would have occurred. MMN peak amplitude and peak latency measures were compared between the 1.5-T and mock scanner experiments to assess the effects of the magnetic field and the BA reduction algorithm on the acquired MMN. Significant correlations between the MMN peak amplitudes recorded at the 1.5-T scanner and those recorded in the mock scanner, and between the MMN peak amplitudes recorded in the mock scanner before and after BA reduction, further validated the BA reduction procedures used in this study.

The frequency MMN generators indicated by the BOLD activation foci in the superior temporal plane are consistent with previous estimations of MMN sources based on dipole analysis of electrical and magnetoencephalographic recordings (Scherg et al., 1989; Giard et al., 1990; 1995; Alho et al., 1998; Opitz et al., 1999; 2002). The observed scalp topography in these studies could be accounted for by assuming one or two temporal generators in each hemisphere, an early generator located in or near primary auditory areas on the superior temporal plane and corresponding to the N1 component (occurring with large frequency changes) and a later generator located more anteriorly and laterally and corresponding to the MMN component. In addition, there is some evidence to suggest that other generators, particularly on the lateral surface of the superior temporal lobe, also contribute to the N1 (Wolpaw and Penry, 1975; Celesia, 1976; Naatanen and Picton, 1987) and to the MMN (Paavilainen et al., 1991; Levanen et al., 1996) responses. It has been suggested that the lateral subcomponents may be larger over the right hemisphere (Wolpaw and Penry, 1975; Levänen et al., 1996), though this finding has not been consistent (Scherg and Von Cramon, 1986). Our results support the idea that generators in the right lateral aspect of the superior temporal gyrus are implicated in processes of frequency deviance detection. However, these generators cannot be attributed with certainty to the N1 or to the MMN component, due to the relatively large frequency changes that occurred. It is possible that some of the observed activation reflects differential refractoriness of N1 generators to the standards and deviants (Butler, 1968; Vaughan and Ritter, 1970).

Some of the BOLD activation observed in the present study may also reflect contributions from generators of the P3a component, which appears in the group-average ERP waveforms as a central positivity following the MMN, with larger amplitudes for the larger deviants (Fig. 3). The P3a is thought to receive contributions from temporal lobe (Alho

Table 2
Peaks of BOLD activation correlated with the magnitude of the ERP negativity during the MMN range[a]

Talairach coordinates (mm)			Anatomical location	BA
x	*y*	*z*		
62	−44	20	Right STG: Posterior dorsal	22
52	−41	7	Posterior ventral	
54	−24	2	Middle ventral	
43	−31	10	Right STP: HG	41
36	−20	6	HG	
52	−14	8	PT	42
53	−26	14	PT	
−49	−29	6	Left STG: Middle ventral	22
−43	−31	16	Left STP: HG	41
−66	−23	13	PT	42

[a] Coordinates in standard stereotaxic space (Talairach and Tournoux, 1988), approximate anatomical locations and Brodmann areas (BA) of activation foci in clusters larger than 300 μl and with *z*-values above 0.03 (uncorrected voxelwise $P < 10^{-8}$) are given. *x*, lateral distance from anterior commissure-posterior commissure (AC-PC) line (positive right); *y*, anterior-posterior distance from AC (positive is in front of AC); *z*, distance above-below AC-PC line (positive is above). Abbreviations: STG, superior temporal gyrus; STP, superior temporal plane; HG, Heschl's Gyrus; PT, planum temporale; BOLD, blood oxygenation level dependent (signal); ERP, event-related potential; MMN, mismatch negativity.

et al., 1998; Escera et al., 1998) and frontal lobe (Knight, 1984) generators. Escera et al., (1998) suggested that there may be two distinct subcomponents contributing to the P3a, early activity of generators in temporoparietal cortex signaling violations of a model of the external world maintained in this area, and later involvement of right frontal lobe generators reflecting orienting of attention triggered by occurrence of a deviant. The lack of frontal BOLD activation foci in the present study suggests that the observed P3a corresponded to the earlier subcomponent described by Escera et al. (1998).

BOLD activation foci observed in a previous fMRI and ERP passive oddball study (Opitz et al., 1999) employing comparable (40%) pure tone frequency changes were restricted to the right and left Heschl's gyri (BA 41). Primary auditory areas on Heschl's gyrus were also activated in the present study, but the bulk of the activation was more lateral and centered in secondary and association auditory areas on the superior temporal gyrus. It is possible that the sensitivity of the present study was enhanced due to the following several methodological differences: (1) A clustered image acquisition paradigm was used, allowing the tones to be presented in relatively quiet periods. (2) Higher spatial resolution was used for image acquisition (16 axial, 4-mm thick, contiguous slices in the present study relative to 7 axial, 6-mm slices with 2-mm interslice gaps in the Opitz study). (3) Two (rather than one in the Opitz study) deviant conditions were used, allowing for more sensitive correlation of the BOLD activation with the magnitude of the deviant.

Similar to our results, frontal BOLD activations were also not observed in the Opitz study (Opitz et al., 1999), though a P3a-like positivity was present in their group-average ERP waveforms. In a follow-up study, Opitz et al. (2002) did observe fronto-opercular BOLD activations to frequency deviations, albeit with complex chord-like tones and with stronger activations for medium (30%) rather than for large (100%) frequency deviations. Interpretation of this frontal activation was complicated by the complexity of the auditory stimuli and their interaction with the noisy scanning environment, and it could not clearly be related to involuntary switching of attention. Our results are consistent with a model whereby the predominant activation underlying frequency deviant detection is centered in the right superior temporal lobe and does not necessarily involve frontal lobe structures, even in conditions with relatively large deviants.

The strong right lateralization of the BOLD activation and of the MMN scalp topography supports the notion of right hemisphere dominance in generation of the frequency MMN (Scherg et al., 1989; Giard et al., 1990; Paavilainen et al., 1991; Naatanen, 1992; Opitz et al., 1999). The asymmetry of BOLD activation suggests that the ERP MMN scalp topography is due at least in part to an asymmetric distribution of auditory temporal MMN generators and is not solely a result of bilateral activation of generators with asymmetric orientations (generators in both hemispheres oriented toward the right) or solely a result of right lateralized activation of a frontal generator (Giard et al., 1990). These results are also consistent with the concept of right hemisphere involvement in fine spectral analysis of sound (Zatorre et al., 1992).

In conclusion, this study demonstrates that a robust BOLD and ERP MMN response can be obtained by using simultaneous recording techniques. The combination of methods revealed detailed information about the generators involved in passive frequency deviant detection. This experimental paradigm can further be used to investigate brain areas involved in other specific aspects of auditory processing.

Acknowledgments

We thank Ed Possing and Tim Thelaner for technical assistance. This study was supported by NIDCD grant R21 DC04880 and by NINDS grant R01 NS33576.

References

Alho, K., 1995. Cerebral generators of mismatch negativity (MMN) and its magnetic counterpart (MMNm) elicited by sound change. Ear Hear. 16, 38–51.

Alho, K., Paavilainen, P., Reinikainen, K., Sams, M., Naatanen, R., 1986. Separability of different negative components of the event-related potential associated with auditory stimulus processing. Psychophysiology 23, 613–623.

Alho, K., Winkler, I., Escera, C., Huotilainen, M., Virtanen, J., Jaaskelainen, I., Pekkonen, E., Ilmoniemi, R., 1998. Processing of novel sounds and frequency changes in the human auditory cortex: magnetoencephalographic recordings. Psychophysiology 35, 211–224.

Allen, P.J., Polizzi, G., Krakow, K., Fish, D.R., Lemieux, L., 1998. Identification of EEG events in the MR scanner: the problem of pulse artifact and a method for its subtraction. Neuroimage 8, 229–239.

Bonmassar, G., Anami, K., Ives, J., Belliveau, J.W., 1999. Visual evoked potential (VEP) measured by simultaneous 64-channel EEG and 3T fMRI. Neuroreport 10, 1893–1897.

Bonmassar, G., Schwartz, D.P., Liu, A.K., Kwong, K.K., Dale, A.M., Belliveau, J.W., 2001. Spatiotemporal brain imaging of visual-evoked activity using interleaved EEG and fMRI recordings. Neuroimage 13, 1035–1043.

Bullmore, E., Brammer, M., Williams, S.C., Rabe-Hesketh, S., Janot, N., David, A., Mellers, J., Howard, R., Sham, P., 1996. Statistical methods of estimation and inference for functional MR image analysis. Magn. Reson. Imaging 35, 261–277.

Butler, R.A., 1968. Effects of changes in stimulus frequency and intensity on habituation of the human vertex potential. J Acoust. Soc. Am. 44, 945–950.

Celesia, G.G., 1976. Organization of auditory cortical areas in man. Brain 99, 403–414.

Cox, R.W., 1996. AFNI: software for analysis and visualization of functional magnetic resonances neuroimages. Comput. Biomed. Res. 29, 162–173.

Cox, R.W., Jesmanovicz, A., 1999. Real-time 3D image registration for functional MRI. Magn. Reson. Med. 42, 1014–1018.

Edmister, W.B., Talavage, T.M., Ledden, P.J., Weisskoff, R.M., 1999. Improved auditory cortex imaging using clustered volume acquisitions. Hum. Brain Mapp. 7, 89–97.

Escera, C., Alho, K., Winkler, I., Naatanen, R., 1998. Neural mechanisms of involuntary attention to acoustic novelty and change. J Cogn. Neurosci. 10, 590–604.

Giard, M.H., Perrin, F., Pernier, J., Bouchet, P., 1990. Brain generators implicated in the processing of auditory stimulus deviance: a topographic event-related potential study. Psychophysiology 27, 627–640.

Giard, M.H., et al., 1995. Separate representation of stimulus frequency, intensity, and duration in auditory sensory memory. J Cogn. Neurosci. 7, 133–143.

Knight, R.T., 1984. Decreased response to novel stimuli after prefrontal lesions in man. Electroencephalogr. Clin. Neurophysiol. 59, 9–20.

Kruggel, F., Herrmann, C.S., Wiggins, C.J., Von Cramon, D.Y., 2001. Hemodynamic and electroencephalographic responses to illusory figures: recording of the evoked potentials during functional MRI. Neuroimage 14, 1327–1336.

Kruggel, F., Wiggins, C.J., Herrmann, C.S., Von Cramon, D.Y., 2000. Recording of the event-related potentials during functional MRI at 3.0 Tesla field strength. Magn. Reson. Imaging 44, 277–282.

Lang, A.H., et al., 1990. Pitch discrimination performance and auditory evoked potentials. In: Brunia, C.H.M., Gaillard, A.W.K., Kok, A. (Eds.), Psychophysical Brain Research. Tilburg University Press, Tilburg, pp. 294–298.

Lang, A.H., Eerola, P., Korpilahti, I., Holopainen, I., Salo, S., Aaltonen, O., 1995. Practical issues in the clinical application of mismatch negativity. Ear Hear. 16, 118–130.

Levänen, S., Ahonen, A., Hari, R., McEvoy, L., Sams, M., 1996. Deviant auditory stimuli activate human left and right auditory cortex differently. Cereb. Cortex 6, 288–296.

Naatanen, R., 1992. Attention and Brain Function. Erlbaum, Hillsdale, NJ.

Naatanen, R., Picton, T., 1987. The N1 wave of the human electric and magnetic response to sound: a review and an analysis of the component structure. Psychophysiology 24, 375–425.

Opitz, B., Mecklinger, A., Von Cramon, D.Y., Kruggel, F., 1999. Combining electrophysiological and hemodynamic measures of the auditory oddball. Psychophysiology 36, 142–147.

Opitz, B., Rinne, T., Mecklinger, A., Von Cramon, D.Y., Schroeger, E., 2002. Differential contribution of frontal and temporal cortices to auditory change detection: fMRI and ERP results. Neuroimage 15, 167–174.

Paavilainen, P., Alho, K., Reinikainen, K., Sams, M., Naatanen, R., 1991. Right hemisphere dominance of different mismatch negativities. Electroencephalogr. Clin. Neurophysiol. 78, 466–479.

Pan, J., Tompkins, W.J., 1985. A real time QRS detection algorithm. IEEE Trans. Biomed. Engin. 32, 230–236.

Scherg, M., Vasjar, J., Picton, T.W., 1989. A source analysis of the late human auditory evoked potentials. J. Cogn. Neurosci. 1, 336–355.

Scherg, M., Von Cramon, D., 1986. Evoked dipole source potentials of the human auditory cortex. Electroencephalogr. Clin. Neurophysiol. 65, 344–360.

Schomer, D.L., Bonmasser, G., Lazeyras, F., Seeck, M., Blum, A., Anami, K., Schwartz, D., Belliveau, J.W., Ives, J., 2000. EEG-linked functional magnetic resonance imaging in epilepsy and cognitive neurophysiology. J Clin. Neurophysiol. 17, 43–58.

Talairach, J., Tournoux, P., 1988. Co-Planar Stereotaxic Atlas of the human Brain. Thieme Medical Publishers, New York.

Tiitinen, H., May, K., Reinikainen, K., Naatanen, R., 1994. Attentive novelty detection in humans is governed by pre-attentive sensory memory. Nature 372, 90–92.

Vaughan Jr., H.G., Ritter, W., 1970. The sources of auditory evoked responses recorded from the human scalp. Electroencephalogr. Clinl. Neurophysiol. 28, 360–367.

Ward, B.D., 2000. Simultaneous inference for fMRI data; http://afni.nimh.nih.gov/afni/docpdf/.

Wolpaw, J.R., Penry, J.K., 1975. A temporal component of the auditory evoked response. Electroencephalogr. Clin. Neurophysiol. 39, 609–620.

Zatorre, R.J., Evans, A.C., Meyer, E., Gjedde, A., 1992. Lateralization of phonetic and pitch discrimination in speech processing. Science 256, 846–848.